Journal of
Reinforced Plastics and Composites

Mechanical and rheological response of polypropylene/boehmite nanocomposites

Journal:	*Journal of Reinforced Plastics and Composites*
Manuscript ID:	Draft
Manuscript Type:	Original Article
Date Submitted by the Author:	n/a
Complete List of Authors:	Pedrazzoli, Diego; University of Trento, Department of Industrial Engineering Tuba, Ferenc; Budapest University of Technology and Economics, Department of Polymer Engineering Khumalo, Vincent; Polymers and Composites, Materials Science and Manufacturing, Council for Scientific and Industrial Research, CSIR Pegoretti, Alessandro; University of Trento, Department of Industrial Engineering Karger-Kocsis, Jozsef; Budapest University of Technology and Economics, Department of Polymer Engineering
Keyword:	Nanocomposites, Mechanical properties, EWF (Essential Work of Fracture), Thermal properties
Abstract:	In this work the influence of synthetic boehmite alumina (BA) nanoparticles with various surface treatments on the morphology, crystallization behavior and mechanical properties of polypropylene copolymer (PP) nanocomposites was studied. In particular, a series of PP/BA nanocomposites, containing up to 10 wt% of untreated and of octylsilane-functionalized BA nanoparticles, were prepared by melt compounding and film blowing. A third type of composites was produced by incorporation of BA nanoparticles treated with benzene-sulfonic-acid. Scanning electron microscopy indicated that BA nanoparticles were finely and uniformly dispersed, though agglomerated, in the PP nanocomposites. Surface treated BA nanoparticles were better dispersed in the matrix than untreated ones. The melt viscosity of nanocomposites remained unaltered or decreased by nanofiller incorporation at low contents (2.5 and 5 wt%), while it slightly increased at higher contents (10 wt%). Uniaxial tensile tests indicated that the nanoparticles can induce a remarkable stiffening effect even at a rather low filler content, especially in the case of surface treated particles. The plane stress fracture toughness of the material, evaluated by the essential work of fracture approach, showed a noticeable improvement due to BA incorporation, with an optimal effect for a filler concentration of about 2.5 wt%.

Journal of Reinforced Plastics & Composites

Mechanical and rheological response of polypropylene/boehmite nanocomposites

D. Pedrazzoli [(a)], F. Tuba [(b)], V. M. Khumalo [(c)], A. Pegoretti [(a)]*, J. Karger-Kocsis [(b,d)]

[(a)] University of Trento, Department of Industrial Engineering and INSTM Research Unit, Via Mesiano 77, 38123 Trento (Italy)

[(b)] Budapest University of Technology and Economics, Faculty of Mechanical Engineering, Department of Polymer Engineering, 1111 Budapest (Hungary)

[(c)] Polymers and Composites, Materials Science and Manufacturing, Council for Scientific and Industrial Research, CSIR, P.O. Box 395, Pretoria 0001, South Africa

[d)] MTA–BME Research Group for Composite Science and Technology, Műegyetem rkp. 3., H-1111 Budapest (Hungary)

*Corresponding author.

Tel.: +39-0461-282452; fax: +39-0461-281977

e-mail address: alessandro.pegoretti@unitn.it

Abstract

In this work the influence of synthetic boehmite alumina (BA) nanoparticles with various surface treatments on the morphology, crystallization behavior and mechanical properties of polypropylene copolymer (PP) nanocomposites was studied. In particular, a series of PP/BA nanocomposites, containing up to 10 wt% of untreated and of octylsilane-functionalized BA nanoparticles, were prepared by melt compounding and film blowing. A third type of composites was produced by incorporation of BA nanoparticles treated with benzene-sulfonic-acid.

Scanning electron microscopy indicated that BA nanoparticles were finely and uniformly dispersed, though agglomerated, in the PP nanocomposites. Surface treated BA nanoparticles were better dispersed in the matrix than untreated ones. The melt viscosity of nanocomposites remained unaltered or decreased by nanofiller incorporation at low contents (2.5 and 5 wt%), while it slightly increased at higher contents (10 wt%). Uniaxial tensile tests indicated that the nanoparticles can induce a remarkable stiffening effect even at a rather low filler content, especially in the case of surface treated particles. The plane stress fracture toughness of the material, evaluated by the essential work of fracture approach, showed a noticeable improvement due to BA incorporation, with an optimal effect for a filler concentration of about 2.5 wt%.

Keywords

Nanocomposite, Mechanical properties, Thermal properties, EWF (Essential Work of Fracture)

1. Introduction

Nanocomposites formed by incorporating organic or inorganic nanofillers in a polymeric matrix are a relatively new class of composite materials. The introduction of nanodispersed particles in low quantities (i.e. less than 5-10 wt%) can remarkably increase the performances of conventional polymeric matrices (Dorigato, 2010; Sengupta et al., 2011; Fu et al., 2008). Improvements in thermal, mechanical, rheological and morphological properties can occur simultaneously (Paul and Robeson, 2008; Sengupta et al., 2011). Furthermore, novel and specific functionalities can be added, such as increased chemical and flame resistance, improved electrical conductivity, barrier properties, dimensional stability and optical homogeneity (Gupta et al., 2010). Interfacial interactions and dispersion level of fillers are key issues in determining the final performance of polymer nanocomposites (Rong et al., 2004; Dorigato et al., 2013).

Isotactic polypropylene (PP) is probably one of the most interesting commodity thermoplastic, widely used in many fields such as automotive, construction and home appliances. In particular, PP is extensively utilized not only for its balanced thermal and mechanical properties, but also due to its environmental friendliness and easy processability at a relatively low cost (Karger-Kocsis, 1999). PP has been also widely used in association with various kinds of nanofillers such as carbon nanotubes and nanofibre (Ma et al., 2010; Wu et al., 2011; Rex J. Kuriger 2002), layered silicates (Ardanuy and Velasco, 2011; Olewnik et al., 2010; Perrinsarazin et al., 2005) and graphites (Kalaitzidou et al., 2007b; Kalaitzidou et al., 2007a; Li and Wu, 2012), nanoparticles such as silica (Pedrazzoli and Pegoretti, 2013; Sengupta et al., 2011) and calcium carbonate (Karamipour et al., 2011; Wang et al., 2010). An important role is played by such inorganic nanofillers, which can be usually dispersed at nanometric level without the addition of compatibilizers. Metal oxides such as ZnO, MgO_2, Al_2O, etc., in their nanocrystalline form have been found to have unique properties when compared to their respective microcrystalline form (Ogunniran et al., 2012). Among inorganic nanofillers, boehmite alumina

(BA), with chemical formula n-AlO(OH), represents an ideal candidate thanks to its economic and relative easy production process (Özdilek et al., 2008). BA has recently become the subject of research attention as a new type of additive for enhancing the mechanical, thermal and fire-retardant performance of polymers. Streller et al. reported how the addition of these highly dispersible particles produced a significant improvement in the mechanical properties of PP (Streller et al., 2008). The incorporation of up to 8 wt% of BA nanoparticles has been proven to induce a remarkable reinforcement of low-density polyethylene and to improve the ductility of high-density polyethylene (HDPE) (Khumalo et al., 2010b; Khumalo et al., 2010a). Halbach et al. studied the effect of BA addition on the mechanical behaviour and morphology of HDPE and poly(ethylene-co-1-octene) thermoplastic elastomers (Halbach and Mülhaupt, 2008; Halbach et al., 2008). In particular, different BAs with variable sizes, shapes, and aspect ratios were considered, showing that stiffness of HDPE improved upon nanofiller addition without negative effects on the elongation at break. In fact, the increase of stiffness was accompanied by a simultaneous increase of the elongation at break. Özdilek et al. studied the effects of both untreated and surface treated BA on the thermo-mechanical properties and polymer morphology in polyamide 6 nanocomposites, showing that the polymer crystalline structure is significantly changed and the storage modulus is practically doubled upon inclusion of BA particles (Özdilek et al., 2005; Özdilek et al., 2008; Tuba et al., 2013a). It was also shown that both types of BA impart the thermo-oxidative stability to the polymer, with a significative increment of the heat distortion temperature. Moreover, Zhang et al. showed how the thermal stability and flame-retardancy properties of polyethylene terephthalate can be highly enhanced upon incorporation of BA nanoparticles (Zhang et al., 2010).

Though PP does not include any polar groups in its backbone that could interact with BA nanoparticles, the latter can be adequately dispersed also without surface treatment and without polymer coupling agents.

Nevertheless, some recent works showed that the organophilic surface treatment of BA particles may improve their dispersion via controlled interfacial adhesion between BA and PP (Streller et al., 2008; Adhikari et al., 2012; Hosseinpour et al., 2005).

Although few reports are present in the current literature, which examine the mechanical and structural properties of PP-BA nanocomposites (Streller et al., 2008), no reports are available to our knowledge on a detailed investigation and comparison of PP matrices added with untreated and surface treated BA nanoparticles. Moreover, the study of material toughness in PP nanocomposites by applying the essential work of fracture (EWF) method still needs to be ascertained (Bárány et al., 2010).

Therefore, the main aim of this work is to investigate the effect of the addition of BA nanoparticles with different surface functionalizations on the morphology, thermal and mechanical properties of a PP matrix. Particular attention is devoted to the study of the material toughness by the application of the EWF method.

2. Experimental section

2.1 Materials and samples preparation

A polypropylene impact copolymer (MFI at 230°C and 2.16 kg = 1.5 g/10', density = 0.905 g·cm^{-3}) with grade CHR 440 was provided by Sasol South Africa (Sasolburg, South Africa). As nanofiller synthetic Disperal®80 boehmite of Sasol GmbH (Hamburg, Germany) has been used. Nano boehmite alumina is typically characterized by an orthorhombic crystalline structure and nanometric-sized crystallites. In particular, boehmite was used in pristine (BA80), and in surface treated forms. The latter occurred by octylsilane (BA80-OS) and by C10–C13 alkylbenzene sulphonic acid (BA80-OS2), respectively. BA was incorporated in 2.5, 5 and 10 wt%. BA80 nanoparticles were characterized by a crystallite size of 74.4 nm,

mean particle size of 80 µm (as measured on the powder), and BET surface area of 88.0 $m^2 \cdot g^{-1}$ (Khumalo et al., 2010b).

Samples were prepared by melt mixing using a Berstorff co-rotating twin-screw extruder (ZE-40, Berstorff, Hannover, Germany) followed by granulation. The barrel temperatures from the hoper to die were 185, 195, 205, 220 °C, the screw rotated at 100 rpm and the melt passed through the extruder in ca. 80 s. The materials were successively blow moulded (Scientific laboratory extruder-film blowing machine, 25 mm extruder type, model LE25-30/CV) in order to produce film sheets with a thickness of about 0.05 mm. The barrel temperatures from the hoper to die were 180, 185, 190, 195, 200 °C, the screw rotated at 65 rpm and the pressure was 21 MPa. The die temperatures were 200, 210, 220 °C. The rolling speed of nip rollers and pulling rollers was 3.1 and 3.8 $m \cdot min^{-1}$, respectively, while the blower pressure was set to 0.4 MPa.

All specimens necessary for the mechanical tests were cut out from the films along the machine direction. Neat matrix was denoted as PP, while nanocomposites were designated indicating the matrix and the amount and type of filler. For instance, a sample filled with 2.5 wt% of BA80-OS nanoparticles was indicated as PP/2.5BA80-OS.

2.2 Experimental techniques

2.2.1 Morphology and X-ray diffraction

Cryogenic fracture surfaces of unfilled PP and PP nanocomposites were observed at various magnifications by using a Zeiss Supra 40 (Berlin, Germany) field emission scanning electron microscope (FESEM), at an acceleration voltage of 1 kV.

X-Ray diffraction analysis were performed through a Rigaku® 3D Max X-Ray diffractometer on both BA80 nanopowder and PP nanocomposites, scanning the samples in a 2θ range between 3° and 67°, at a 2θ step of 0.1°. The wavelength of the X-Ray source was 0.15418 nm.

2.2.2 Rheology measurements

The melt rheology of the nanocomposites was analyzed by a Rheoplus 32 V3 dynamic oscillatory rheometer (Anton Paar Physics, Ostfildern, Germany) working under controlled strain conditions. The test geometry was cone-plate (cone angle=1°) with a cone diameter of 25 mm. Disk specimens of around 0.6 mm thickness were obtained by overlapping several films. The gap was set at 0.5 mm by squeezing the PP disks. Frequency sweep tests were carried out at T =180°C. During the measurement a small strain amplitude (1%) oscillatory shear was applied to the samples. The storage and loss shear moduli (G' and G'', respectively) and the dynamic complex viscosity $|\eta^*|$ were measured as a function of angular frequency (ω) in the range 0.01–100 rad/s.

2.2.3 Thermal analyses

Differential scanning calorimetry (DSC) tests were carried out by a DSC Q2000 (TA Instruments-Waters LLC, New Castle, USA) differential scanning calorimeter under a constant nitrogen flow of 50 ml·min^{-1}. The samples were heated up to 200 °C at a rate of 10 °C·min^{-1} with subsequent crystallization test down to 0 °C setting a cooling rate of 10 °C·min^{-1}. A subsequent heating scan was performed at 10 °C·min^{-1}. The melting enthalpy of 100% crystalline PP has been considered as ΔH^0 = 209 J·g^{-1} (James, 1999). Moreover, the crystallinity χ_c of nanocomposite samples was calculated by taking the actual weight fraction of PP in the composite into account. The melting temperatures T_{m1} and T_{m2} were recorded during the first and second

heating scan, respectively. The crystallization enthalpy ΔH_c was measured by integrating the heat flow curve during the cooling scan.

Thermogravimetric analyses (TGA) were carried out through a Q5000 IR thermogravimetric analyzer (TA Instruments-Waters LLC, New Castle, USA) imposing a temperature ramp between 40 and 700 °C at a heating rate of 10 °C·min^{-1} under a constant nitrogen flow of 25 ml·min^{-1}. The onset of degradation temperature ($T_{d,onset}$) was determined by the point of intersection of tangents to two branches of the thermogravimetric curve, while the maximum rate of degradation temperature ($T_{d,max}$) was determined from the peak maxima in the first derivative of weight loss curve.

2.2.4 Mechanical tests

Uniaxial tensile tests were performed with a Zwick® Z005 (Zwick GmbH & Co. KG, Germany) universal testing machine. According to ASTM standard D882-10, tests were performed on samples of at least five specimens of rectangular shape with dimension 300 x 15 x 0.05 mm^3. Tests were carried out at a crosshead speed of 25 mm·min^{-1}, with a grip distance of 250 mm. The strain was recorded by a ME-46 Full Image Videoextensometer (Messphysik Laborgeräte GES.m.b.H., Austria) setting a gage length of 40.0 mm, up to a maximum axial deformation of 1%. The elastic modulus was measured as secant modulus between deformation levels of 0.05 % and 0.25 % in according to ISO 527 standard. Uniaxial tensile properties, such as stress at yield (σ_y), stress at break (σ_b) and strain at break (ε_b) were determined at a higher crosshead speed (500 mm·min^{-1}) on specimens of rectangular shape with dimensions of 100 x 15 x 0.05 mm^3, setting an initial distance between the grips of 50 mm and without using the visual extensometer.

Both creep and dynamic mechanical thermal analysis (DMTA) tests were performed utilizing a dynamic mechanical analyzer DMA Q800 (TA Instruments®-Waters LLC, New Castle, USA) on rectangular

specimens with dimensions of 25 x 5 x 0.05 mm^3 adopting a gage length of 11.5 mm. Tensile creep tests were performed under a constant stress (σ_0) of 4 MPa (i.e about 10% of the stress at yield of unfilled PP) for 3600 s at 30 °C. The creep compliance *D(t)*, computed as the ratio between the strain and the creep stress, was plotted against the loading time.

DMTA tests were performed in a temperature range between -40 °C and 160 °C, at a heating rate of 3 °C·min^{-1} and a frequency of 1 Hz. A preload of 0.2 MPa and a maximum strain of 0.05 % were set for each test. The most important viscoelastic functions (*E', E", tanδ*) were recorded.

For the essential work of fracture (EWF) tests, double edge notched tensile (DENT) specimens, having a width (*w*) of 40 mm and a length of 80 mm (clamped length 40 mm), were used. The notches were prepared by razor blades (sliding method) and were perpendicular to the machine direction. The ligament length (*L*) was measured by a profile projector, a magnification of 15x was used. Nominal ligament lengths of 5, 7, 9, 11, 13 and 15 mm were used (five specimens each). The thickness (*B*) of samples was measured by a Mitutoyo micrometer (accuracy: 0.001 mm).

The fracture tests were performed at ambient conditions (24±0.5°C, RH=40±5%) by an Instron 4502 (Instron, Norwood, USA) universal testing machine. The crosshead speed was set to 10 mm·min^{-1}, the displacement values (*x*) were calculated from crosshead travel, while the load (*F*) was recorded by a 100 N load cell. The validity of EWF method (Bárány et al., 2010) was confirmed by:

- the self-similarity of load-displacement curves,
- a check on the ligament yielding – method described in ref (Tuba et al., 2013b),
- a lower ligament limit (L=5 mm), which ensures quasi plane-stress conditions and steady-state crack propagation; determined as outlined previously in (Tuba et al., 2012),

- a confined plastic zone, which was ensured by the condition $L < x_p$, where x_p is the estimated size of the plastic zone based on Cotterell's study (Cotterell et al., 2005). The other generally used criteria (i.e. L<w/3) seem to be too conservative, therefore L=15 mm was used as the upper ligament length limit.

According to EWF approach, the total fracture work (W_f) can be divided in two parts: a work (W_p) dissipated in the outer plastic zone and a work (W_e) essential for the formation of new crack surfaces. The essential fracture work is assumed to be related to the cross-section, LB; while the plastic work to the plastic volume, $\beta L^2 B$. The EWF parameters can be estimated from the linear regression of specific fracture work (w_f) versus ligament length plots by Equation 1.

$$w_f = w_e + \beta w_p L, \quad (1)$$

where $w_f=W_f/LB$, $w_e=W_e/LB$, is the specific essential work of fracture, $w_p=W_p/L^2B$ is the specific plastic work of fracture and β is a geometry dependent correction factor.

3. Results and discussion

3.1 Morphology

The morphology of nanocomposites was examined by means of SEM analyses. In particular, SEM micrographs of PP containing the same amount (2.5 wt%) of BA80, BA80-OS and BA80-OS2 nanoparticles, are reported in Figure 1.

Also in absence of a surface treatment, the shear forces developing in the melt compounder seem to be enough to achieve a quite good deagglomeration and a uniform dispersion of BA nanoparticles. In fact, nanofiller appears quite well dispersed in PP/2.5BA80 nanocomposite, although some aggregates and agglomerates are recognizable. The dispersed nanoboehmites are organized in agglomerates with average

sizes of 400–500 nm composed of the much smaller crystallites (Figure 1a). Moreover, some larger humps and cavities are visible on the fracture surface which can be traced to the rubber (ethylene-propylene) phase of the PP copolymer used.

On the other hand, the silane coupling agent present on the surface of BA80-OS nanoparticles slightly improves the filler dispersion in the polymer matrix (Figure 1b), leading to the presence of smaller and more uniformly distributed BA aggregates. Furthermore, a better polymer–filler adhesion takes place due to replacement of hydroxide groups on the surface of nanoparticles with organic groups (Brostow et al., 2009), showing much less cavities due to detachment of aggregate and agglomerates. A similar filler dispersion is recognizable in the case of BA nanoparticles surface treated with benzene-sulfonic acid (carrying apolar tails), probably because of the higher hydrophobicity of the BA which indicates a lower tendency to filler aggregation (Figure 1c) (Adhikari et al., 2012).

The XRD diffractogram of BA80 nanopowder, PP, and related nanocomposites are reported in Figure 2. X-ray diffractogram of BA80 nanopowder puts into evidence the presence of two main BA crystals by identification of diffraction reflections (hkl plan) at 2θ=14.7°(020) and 2θ=28.4°(120). The average crystallite size, calculated by the Scherrer's equation (Azároff, 1968), is about 72.2 nm, in accordance with the data reported on the material datasheet (Khumalo et al., 2010b). According to XRD diffractograms of PP nanocomposites, the two reflections of BA (i.e. 2θ=14.7°, 2θ=28.4°) are recognizable and their intensity increases with the nanofiller amount.

Moreover, XRD diffractograms of neat PP and related nanocomposites present the typical signals of the α-crystalline form (2θ=14.0°, 2θ=16.8°, 2θ=18.6°, 2θ=21.2°, 2θ=21.8°), while limited and sporadic occurrence of β-modification (2θ=16.1°) and γ-modification (2θ=20.1°) can be observed. The diffractograms of PP nanocomposites generally indicate a slightly higher matrix crystallinity when nanofillers are dispersed, in

accordance with the crystallinity values measured through DSC analysis (see Table 1). In particular, the diffraction intensity of the PP peaks slightly increases after the incorporation of BA particles, although the peak at 2θ=16.8° seems to change without any evident dependence upon the filler content. The reason of this finding is not clear to the authors yet.

3.2 Rheological characterization

The frequency dependence at isothermal conditions of the dynamic shear storage modulus (G') and complex viscosity ($|\eta^*|$) are plotted in Figure 3a for neat PP and PP composites filled with 2.5 wt% of both untreated and surface treated BA nanoparticles. It is interesting to observe that both G' and $|\eta^*|$ values are quite similar when neat PP and nanocomposites filled with surface treated BA nanoparticles are compared. On the other hand, a general decrease in both G' and $|\eta^*|$ can be easily detected for the system modified with untreated BA over the whole frequency range. Noteworthy, the reduction in viscosity is surely beneficial for the material processing. In one of our previous work, we showed how the addition of both untreated and surface treated BA particles with an average crystallite size of 40 nm to a LLDPE matrix induced a decrease in both G' and $|\eta^*|$ compared to that of unfilled LLDPE (Pedrazzoli et al., 2013). Furthermore it was shown that a similar decrease in viscosity is obtained in the case of LLDPE systems modified with untreated BA with higher crystallite size (74 nm). Also Blaszczak et al. studied the rheological behaviour of LDPE-BA nanocomposite and found that the addition of BA produces a decrease in $|\eta^*|$ compared to that of unfilled LDPE (Blaszczak et al., 2010). A viscosity decrease is recorded in PP samples filled with untreated BA, probably because even these BA particles may affect the chain entangling in the melt. Furthermore, micrograph images obtained by ESEM on PP/2.5BA80-OS and PP/2.5BA80-OS2 samples show that matrix-filler adhesion is improved by

surface functionalization of BA particles. As a result of better adhesion, the melt of filled polymer becomes more viscous.

Nevertheless, while a similar viscosity to that of unfilled PP is obtained for nanocomposites at 5 wt% BA, an increase in both G' and $|\eta^*|$ is recorded in the case of composites filled with 10 wt% BA (Figure 3b), probably because the nanofiller loading is sufficiently high that nanoparticles begin to interact each others.

3.3 Thermal analyses

The most relevant parameters from DSC analysis are summarized in Table 1. It is worthwhile to observe that the addition of BA nanoparticles produces a slight increase in the crystallization peak temperature irrespective to the boehmite type. The related effect becomes more pronounced at 10 wt% filling. Nevertheless, no particular dependence upon the filler surface treatment can be determined. The nucleating effect of BA was already reported in previous papers on LDPE and HDPE (Khumalo et al., 2010b) and PP (Streller et al., 2008) matrices, with a different nucleating efficiency depending on the crystallite size of boehmite nanofiller.

While the melting temperature recorded during the second scan (T_{m2}) on nanocomposites is quite similar to that of unfilled PP, the crystallinity (χ_c) increases from 37.0% up to 40.7 and 41.1% after adding 10 wt% BA80 and 10 wt% BA80-OS, respectively. These results further indicate that BA may act as nucleation sites for the crystallization of PP. Streller et al. studied the crystallization behavior of PP nanocomposites based upon BA, founding that the degree of crystallinity was not significantly affected by BA addition, but a much larger number and higher density of spherulites was observable by means of polarization optical microscopy on molten samples which were cooled down (Streller et al., 2008).

The thermal stability parameters as detected by TGA measurements are reported in Table 2. When considering PP-BA nanocomposites, both $T_{d,onset}$ and $T_{d,max}$ increase with the filler content. This could also be

mainly attributed to the dehydration process of BA nanofiller which delays the polymer degradation (Zhang et al., 2010). The char content at 700 °C is also shown in Table 2 for all the samples. Improved thermal and thermo-oxidative stability due to the addition of BA has been already reported for polyethylenes (Khumalo et al., 2010b) and PP (Streller et al., 2008; Bocchini et al., 2007). In one of our previous work we observed a remarkable improvement in thermal resistance parameters with the incorporation of BA in LLDPE matrix, noticing a slight dependence on the BA crystallite size (Pedrazzoli et al., 2013).

3.4 Mechanical testing

The tensile modulus of PP improved with the BA content, showing an improvement of about 46% for systems filled with 10 wt% of BA80-OS (see Table 3). Moreover, both surface treated BA nanoparticles seem to have a better efficiency in increasing the stiffness of PP with respect to untreated BA.

In general, yield stress and stress at break values slightly decrease with the addition of untreated BA, probably due to filler agglomeration (Brostow et al., 2009). Interestingly, since the decrease in yield stress measured on bulk samples is accompanied by a lower viscosity of the melt polymer, BA nanoparticles might act as a solid-phase plasticizer.

Filler agglomeration is also supposed to be responsible for the decrease in the elongation at break of nanocomposites with respect to the neat matrix, showing the behavior often reported for polymer nanocomposites filled with inorganic fillers. It is worthwhile to note that the stress at yield, stress at break and strain at break values of PP/BA80-OS nanocomposites are higher than those of PP/BA80 at the same filler weight content. These results suggest that the utilization of surface treated BA is essential to achieve higher strength and stiffness at low nanofiller concentrations. Brostow et al. studied the tensile properties and properties at the interface of low density polyethylene (LDPE) filled with untreated and silane functionalized

BA nanoparticles (Brostow et al., 2009). In his work it was shown that the strain at break increases with a silane treatment and decreases with an increment of filler loading, indicating that the silane coupling agent present on the surface of BA probably provides a lubricating or plasticizing effect.

Furthermore, the sample PP/2.5BA80-OS2 shows lower ultimate tensile properties with respect to PP/2.5BA80 and PP/2.5BA80-OS samples. Although an increase was expected as a result of smaller agglomerations, which could act as stress concentrators of failure points, however, this was not the case. In prticular, the remarkable decrease in the elongation at break might be attributed to the rigidity of the benzene group present on the filler surface and characterizing the polymer-matrix interface.

In Figure 4a and Figure 4b the isothermal creep compliance of unfilled PP and PP nanocomposites filled with 2.5 wt% BA and 5 and 10 wt% BA, under a constant load of 4 MPa and at 30 °C, is represented, respectively. The elastic (D_e) and total components of the creep compliance after 2000 s (D_{t2000}) are summarized in Table 4. The introduction of BA nanoparticles leads to a significant improvement of the creep stability of the material. It is generally believed that nanoparticles can effectively restrict the motion of polymer chains, thus influencing the stress transfer at a nanoscale, with positive effects on the creep stability of the material (Kolarik and Pegoretti, 2006). Although creep compliance data of nanocomposites filled with 2.5 wt% BA does not show any significant difference, the addition of BA80-OS gives better creep stability than BA80 at 5 and 10 wt%, showing a dependence on the BA surface functionalization. The better filler dispersion and the apolarity achieved with surface treated BA particles not only produces higher stiffness, but also promotes a more efficient stress transfer between filler and matrix whereby strongly limiting the viscous flow.

The dynamic storage modulus (*E'*) increases remarkably with increasing BA content (Table 4), indicating that the incorporation of rigid BA nanoparticles produces a reinforcing effect. Furthermore, increase in storage modulus for the nanocomposites with surface treated BA (i.e. PP/BA80-OS and PP/BA80-OS2) is much higher than that of nanocomposites containing untreated BA (i.e. PP/BA80). These results are in good agreement with the modulus improvement observed in quasi-static tensile tests and with the improvements observed during the creep tests. Comparison plots of the storage modulus (*E'*) and loss factor ($tan\delta$) are reported in Figure 5a and Figure 5b, respectively, as a function of temperature for unfilled PP and relative nanocomposites containing 5 and 10 wt% BA. The glass transition temperature (T_g), as detected from the $tan\delta$ peak, slightly increased in nanocomposites of higher filler content with respect to unfilled PP, reflecting the restriction of the motion of polymer chains induced by the nanofillers incorporation. It is well known that the T_g of a polymer depends on the mobility of the chain segment of the macromolecules in the polymer matrix. If the molecular chain is restricted, motion or relaxation of the chain segment becomes difficult at the original glass transition temperature and a higher temperature is required (Prashantha, 2011). Therefore, the increase in T_g values may be related to the degree of the homogeneous dispersion of nanoparticles in the polymer matrix and the interactions between the filler and polymer (Rong et al., 2004).

During the facture studies, the correlation coefficients (R^2) of EWF tests varied between 0.96 and 0.99, while the standard deviation values scattered between 3 and 6.5 $kJ \cdot m^{-2}$, for all samples. Based on previous studies of Williams and Rink (Williams and Rink, 2007), and Tuba et al. (Tuba et al., 2011), these results are adequate for an accurate application of the EWF approach. A minimum sample size (N) of 25 ensured the accuracy of the measurements (Pegoretti et al., 2009).

The specific essential work of fracture (w_e) of PP increases after the incorporation of boehmite alumina (Figure 6). As the crystalline morphology did not change significantly (see Table 1), this reinforcing effect can be mainly attributed to the nanofiller. Nevertheless, an increasing filler content induces a reduction of w_e values (Table 5), which is a general observation for "over-filled" nanocomposites and can be attributed to the agglomeration of nanoparticles. This disadvantageous effect caused the decrease of yield-stress (see Table 3), too. Although the OS treatment results in increasing yield stress at low filler content; the w_e term does not increase further, and what is even more interesting, it decreases. This observation is in good agreement with the observation of Arkhireyeva and Hashemi (Arkhireyeva and Hashemi, 2002) regarding the direct proportion between w_e and $e_0 \cdot \sigma_y$, where e_0 is the ordinate intercept of extension at break (DENT specimens) versus ligament length linear regression plots.

The nanocomposites have smaller plastic work of fracture, βw_p, compared to the neat PP material. The increasing filler content also results in decreasing βw_p values. However, the w_p terms of the examined nanocomposites, except that of PP/2.5BA80 composite, do not differ significantly (p=0.05), thus the dissipative plastic work was not influenced by the nanofillers.

4. Conclusions

PP based composites were prepared by melt compounding and film blowing using both untreated and surface treated BA nanoparticles up to filler contents of 10 wt% in order to assess the role of filler content and surface treatment on the thermal, mechanical and rheological properties of the resulting composites.

The addition of surface treated nanoparticles resulted in a better dispersion of the filler within the matrix, as confirmed by SEM and TEM observations. BA acted as a weak nucleating agent, producing a slight increase of the crystallization peak temperature. The melt viscosity of nanocomposites remained unaltered or

decreased by nanofiller incorporation at low contents (2.5 and 5 wt%), while it slightly increased at higher contents (10 wt%). BA incorporation enhanced the resistance to thermal degradation of the PP matrix.

The mechanical properties of all samples were characterized by tensile, creep, dynamic mechanical thermal analysis and mode I-type fracture tests. The results of tensile tests indicated that the nanoparticles can stiffen PP even at a low filler content, especially in the case of treated BA, without a significative loss in ductility. Increasing stiffening was, however, accompanied with decreasing yield stress and elongation at yield.

Creep tests showed that creep compliance was remarkably reduced by nanofiller incorporation. Both storage and loss modulus were enhanced in all nanocomposites demonstrating the reinforcing effect of the BA particles.

Finally, the toughness of the material, evaluated through EWF approach, showed an improvement indicated by a rise of specific essential work of fracture values due to BA incorporation, with a decline occurring at higher filler contents because of nanofiller agglomeration.

Acknowledgements

This work was performed in the framework of a bilateral cooperation agreement between Italy and Hungary (HU11MO8).

The authors greatly acknowledge Prof. Riccardo Ceccato of the Department of Industrial Engineering of the University of Trento for his kind assistance in XRD analyses and rheological measurements.

References

Adhikari R, Brostow W, Datashvili T, et al. (2012) Effect of surfactant treated boehmite nanoparticles on properties of block copolymers. *Materials Research Innovations* 16: 19-24.

Ardanuy M and Velasco JI. (2011) Mg–Al Layered double hydroxide nanoparticles. *Applied Clay Science* 51: 341-347.

Arkhireyeva A and Hashemi S. (2002) Combined effect of temperature and thickness on work of fracture parameters of unplasticized PVC film. *Polymer Engineering & Science* 42: 504-518.

Azároff LV. (1968) Chapter 9. *Elements of X-Ray Crystallography.* New York: McGraw-Hill Education.

Bárány T, Czigány T and Karger-Kocsis J. (2010) Application of the essential work of fracture (EWF) concept for polymers, related blends and composites: A review. *Progress in Polymer Science* 35: 1257-1287.

Blaszczak P, Brostow W, Datashvili T, et al. (2010) Rheology of low-density polyethylene + Boehmite composites. *Polymer Composites* 31: 1909-1913.

Bocchini S, Morlat-Thérias S, Gardette J-L, et al. (2007) Influence of nanodispersed boehmite on polypropylene photooxidation. *Polymer Degradation and Stability* 92: 1847-1856.

Brostow W, Datashvili T, Huang B, et al. (2009) Tensile properties of LDPE + Boehmite composites. *Polymer Composites* 30: 760-767.

Cotterell B, Pardoen T and Atkins AG. (2005) Measuring toughness and the cohesive stress-displacement relationship by the essential work of fracture concept. *Engineering Fracture Mechanics* 72: 827-848.

Dorigato A. (2010) Linear low-density polyethylene/silica micro- and nanocomposites: dynamic rheological measurements and modelling. *eXPRESS Polymer Letters* 4: 115-129.

Dorigato A, Dzenis Y and Pegoretti A. (2013) Filler aggregation as a reinforcement mechanism in polymer nanocomposites. *Mechanics of Materials* 61: 79-90.

Fu S, Feng X, Lauke B, et al. (2008) Effects of particle size, particle/matrix interface adhesion and particle loading on mechanical properties of particulate–polymer composites. *Composites Part B: Engineering* 39: 933-961.

Gupta RK, Kennel E and Kim K-J. (2010) Polymer Nanocomposites Handbook. Boca Raton, FL: CRC Press.

Halbach TS and Mülhaupt R. (2008) Boehmite-based polyethylene nanocomposites prepared by in-situ polymerization. *Polymer* 49: 867-876.

Halbach TS, Thomann Y and Mülhaupt R. (2008) Boehmite nanorod-reinforced-polyethylenes and ethylene/1-octene thermoplastic elastomer nanocomposites prepared byin situ olefin polymerization and melt compounding. *Journal of Polymer Science Part A: Polymer Chemistry* 46: 2755-2765.

Hosseinpour D, Guthrie JT, Berg JC, et al. (2005) The effect of interfacial interaction contribution to the mechanical properties of automotive topcoats. *Progress in Organic Coatings* 54: 182-187.

James E. (1999) *Polymer data handbook,* New York: Oxford University Press.

Kalaitzidou K, Fukushima H and Drzal LT. (2007a) Multifunctional polypropylene composites produced by incorporation of exfoliated graphite nanoplatelets. *Carbon* 45: 1446-1452.

Kalaitzidou K, Fukushima H and Drzal LT. (2007b) A new compounding method for exfoliated graphite–polypropylene nanocomposites with enhanced flexural properties and lower percolation threshold. *Composites Science and Technology* 67: 2045-2051.

Karamipour S, Ebadi-Dehaghani H, Ashouri D, et al. (2011) Effect of nano-CaCO3 on rheological and dynamic mechanical properties of polypropylene: Experiments and models. *Polymer Testing* 30: 110-117.

Karger-Kocsis J. (1999) Polypropylene: an A-Z reference. Dordrecht, The Netherlands: Kluwer Publishers.

Khumalo VM, Karger-Kocsis J and Thomann R. (2010a) Polyethylene/synthetic boehmite alumina nanocomposites: structure, mechanical, and perforation impact properties. *Journal of Materials Science* 46: 422-428.

Khumalo VM, Karger-Kocsis J and Thomann R. (2010b) Polyethylene/synthetic boehmite alumina nanocomposites: Structure, thermal and rheological properties. *eXPRESS Polymer Letters* 4: 264-274.

Kolarik J and Pegoretti A. (2006) Non-linear tensile creep of polypropylene: Time-strain superposition and creep prediction. *Polymer* 47: 346-356.

Li M and Wu Z. (2012) A review of intercalation composite phase change material: Preparation, structure and properties. *Renewable and Sustainable Energy Reviews* 16: 2094-2101.

Ma P-C, Siddiqui NA, Marom G, et al. (2010) Dispersion and functionalization of carbon nanotubes for polymer-based nanocomposites: A review. *Composites Part A: Applied Science and Manufacturing* 41: 1345-1367.

Ogunniran ES, Sadiku R, Sinha Ray S, et al. (2012) Effect of Boehmite Alumina Nanofiller Incorporation on the Morphology and Thermal Properties of Functionalized Poly(propylene)/Polyamide 12 Blends. *Macromolecular Materials and Engineering* 297: 237-248.

Olewnik E, Garman K and Czerwiński W. (2010) Thermal properties of new composites based on nanoclay, polyethylene and polypropylene. *Journal of Thermal Analysis and Calorimetry* 101: 323-329.

Özdilek C, Kazimierczak K and Picken SJ. (2005) Preparation and characterization of titanate-modified Boehmite–polyamide-6 nanocomposites. *Polymer* 46: 6025-6034.

Özdilek C, Norder B and Picken SJ. (2008) A study of the thermo-mechanical behavior of Boehmite-polyamide-6 nanocomposites. *Thermochimica Acta* 472: 31-37.

Paul DR and Robeson LM. (2008) Polymer nanotechnology: Nanocomposites. *Polymer* 49: 3187-3204.

Pedrazzoli D, Ceccato R, Karger-Kocsis J, et al. (2013) Viscoelastic behaviour and fracture toughness of linear-low-density polyethylene reinforced
with synthetic boehmite alumina nanoparticles. *eXPRESS Polymer Letters* 7.

Pedrazzoli D and Pegoretti A. (2013) Silica nanoparticles as coupling agents for polypropylene/glass composites. *Composites Science and Technology* 76: 77-83.

Pegoretti A, Castellani L, Franchini L, et al. (2009) On the essential work of fracture of linear low-density-polyethylene. I. Precision of the testing method. *Engineering Fracture Mechanics* 76: 2788-2798.

Perrinsarazin F, Tonthat M, Bureau M, et al. (2005) Micro- and nano-structure in polypropylene/clay nanocomposites. *Polymer* 46: 11624-11634.

Prashantha K. (2011) Processing and characterization of halloysite nanotubes filled polypropylene nanocomposites based on a masterbatch route: effect of halloysites treatment on structural and mechanical properties. *eXPRESS Polymer Letters* 5: 295-307.

Rex J. Kuriger MKA, David P. Anderson , Ronald L. Jacobsenc (2002) Processing and characterization of aligned vapor grown carbon fiber reinforced polypropylene *Composites Part A: Applied Science and Manufacturing*.

Rong MZ, Zhang MQ, Pan SL, et al. (2004) Analysis of the interfacial interactions in polypropylene/silica nanocomposites. *Polymer International* 53: 176-183.

Sengupta R, Bhattacharya M, Bandyopadhyay S, et al. (2011) A review on the mechanical and electrical properties of graphite and modified graphite reinforced polymer composites. *Progress in Polymer Science* 36: 638-670.

Streller RC, Thomann R, Torno O, et al. (2008) Isotactic Poly(propylene) Nanocomposites Based upon Boehmite Nanofillers. *Macromolecular Materials and Engineering* 293: 218-227.

Tuba F, Khumalo VM and Karger-Kocsis J. (2013a) Essential Work of Fracture of Poly(ϵ-Caprolactone)/Boehmite Alumina Nanocomposites: Effect of Surface Coating. *Journal of Applied Polymer Science*.

Tuba F, Oláh L and Nagy P. (2011) Essential work of fracture study of polymers: a novel criterion for the validation of tested ligament range. *Journal of Materials Science* 46: 7901-7904.

Tuba F, Oláh L and Nagy P. (2012) The role of ultimate elongation in the determination of valid ligament range of essential work of fracture tests. *Journal of Materials Science* 47: 2228-2233.

Tuba F, Oláh L and Nagy P. (2013b) On the valid ligament range of specimens for the Essential Work of Fracture method: the inconsequence of stress criteria. *Engineering Fracture Mechanics* 99: 349-355.

Wang Y, Shen H, Li G, et al. (2010) Crystallization and melting behavior of PP/CaCO3 nanocomposites during thermo-oxidative degradation. *Journal of Thermal Analysis Calorimetry* 100: 999-1008.

Williams JG and Rink M. (2007) The standardisation of the EWF test. *Engineering Fracture Mechanics* 74: 1009-1017.

Wu J, Xiang F, Han L, et al. (2011) Effects of carbon nanotubes on glass transition and crystallization behaviors in immiscible polystyrene/polypropylene blends. *Polymer Engineering & Science* 51: 585-591.

Zhang J, Ji Q, Zhang P, et al. (2010) Thermal stability and flame-retardancy mechanism of poly(ethylene terephthalate)/boehmite nanocomposites. *Polymer Degradation and Stability* 95: 1211-1218.

Figure captions

Figure 1. FESEM images of the fracture surface of (a) PP/2.5BA80, (b) PP/2.5BA80-OS and (c) PP/2.5BA80-OS2 nanocomposites.

Figure 2. XRD diffractogram of BA80 nanopowder and PP nanocomposites filled with 2.5 and 10 wt% BA in comparison.

Figure 3. Complex viscosity $|\eta^*|$ and storage shear modulus (G') with respect to angular frequency (ω) for (a) PP and PP nanocomposites filled with 2.5 wt% BA and (b) PP and PP nanocomposites filled with 5 and 10 wt%.

Figure 4. Creep compliance (D(t)) of neat PP and relative nanocomposites (T=30 °C, $\sigma_0 = 4$ MPa).

Figure 5. Dynamic mechanical properties of neat PP and relative nanocomposites (f = 1 Hz): (a) storage modulus (E') and (b) loss tangent ($tan\delta$).

Figure 6. Specific work of fracture vs. ligament length plots for neat PP and relative nanocomposites.

Table 1. Melting and crystallization characteristics of unfilled PP and relative nanocomposites from DSC measurements.

Sample	T_{m1} [°C]	ΔH_{m1} [J/g] (χ_{m1} [%])	T_c [°C]	ΔH_c [J/g] (χ_c [%])	T_{m2} [°C]	ΔH_{m2} [J/g] (χ_{m2} [%])
PP	162.2	72.3 (34.6)	124.4	78.3 (37.5)	164.3	77.2 (37.0)
PP/2.5BA80	163.5	72.9 (35.8)	125.5	79.5 (39.0)	165.0	77.2 (37.9)
PP/5BA80	162.6	73.8 (37.2)	125.3	78.5 (39.5)	164.4	76.0 (38.3)
PP/10BA80	163.1	72.8 (38.7)	127.7	79.6 (42.3)	165.0	76.6 (40.7)
PP/2.5BA80-OS	163.3	73.3 (36.0)	125.4	79.1 (38.8)	165.0	78.7 (38.6)
PP/5BA80-OS	163.0	73.6 (37.1)	125.3	79.4 (40.0)	164.8	75.7 (38.1)
PP/10BA80-OS	163.4	73.1 (38.9)	128.7	79.9 (42.5)	165.2	77.4 (41.1)
PP/2.5BA80-OS2	163.8	73.4 (36.0)	123.4	78.6 (38.6)	164.1	77.1 (37.8)

Table 2. TGA parameters on unfilled PP and relative nanocomposites.

Sample	$T_{d,\ onset}$ [°C]	$T_{d,\ max}$ [°C]	Char [%]
PP	441.2	461.8	0.25
PP/2.5BA80	441.6	462.9	2.86
PP/5BA80	445.2	466.1	4.79
PP/10BA80	449.0	468.8	9.82
PP/2.5BA80-OS	442.5	463.1	2.90
PP/5BA80-OS	446.1	466.3	4.84
PP/10BA80-OS	449.3	468.7	9.93
PP/2.5BA80-OS2	442.4	462.8	2.96

Table 3. Quasi-static tensile properties at yield and at break of unfilled PP and relative nanocomposites.

Sample	Tensile modulus [MPa]	Tensile strength at yield [MPa]	Tensile stress at break [MPa]	Elongation at break [%]
PP	1426 ± 19	25.2 ± 0.7	40.0 ± 1.4	711 ± 32
PP/2.5BA80	1614 ± 63	23.9 ± 0.6	28.9 ± 1.0	601 ± 32
PP/5BA80	1646 ± 39	23.8 ± 0.7	23.1 ± 0.5	490 ± 81
PP/10BA80	1984 ± 69	17.2 ± 0.5	17.8 ± 0.3	13 ± 1
PP/2.5BA80-OS	1671 ± 45	28.0 ± 1.4	31.5 ± 0.8	641 ± 41
PP/5BA80-OS	1712 ± 49	25.2 ± 0.4	25.6 ± 0.5	600 ± 66
PP/10BA80-OS	2090 ± 23	20.9 ± 0.5	20.6 ± 0.8	30 ± 2
PP/2.5BA80-OS2	1644 ± 62	22.0 ± 0.3	27.5 ± 0.7	31 ± 4

Table 4. Creep compliance data (T=30 °C, σ_0 = 4 MPa) and dynamic mechanical properties of PP and relative nanocomposites (f = 1 Hz).

Sample	D_e [GPa^{-1}]	$D_{ve,2000s}$ [GPa^{-1}]	$D_{tot,2000s}$ [GPa^{-1}]	E' (-40 °C) [MPa]	E' (23 °C) [MPa]	E" (23 °C) [MPa]	T_g [°C]
PP	1.13	0.79	1.92	2601.7	1506.1	70.5	11.6
PP/2.5BA80	0.86	0.62	1.48	3020.0	1619.9	73.7	11.6
PP/5BA80	0.83	0.63	1.46	3325.3	1728.9	74.1	11.7
PP/10BA80	0.78	0.55	1.33	3503.6	2004.0	79.0	12.0
PP/2.5BA80-OS	0.91	0.54	1.45	3139.9	1737.3	71.2	11.9
PP/5BA80-OS	0.80	0.48	1.28	3415.2	1883.5	75.7	12.2
PP/10BA80-OS	0.78	0.36	1.14	3713.5	2251.7	87.0	13.3
PP/2.5BA80-OS2	0.84	0.66	1.50	3204.9	1859.3	74.1	12.0

Table 5. Specific EWF parameters of PP and relative nanocomposites (for w_e and βw_p the 95% confidence limits are indicated).

Sample	w_e [kJ·m^{-2}]	βw_p [MJ·m^{-3}]	β [–]	w_p [MJ·m^{-3}]	e_0 [mm]	R^2 [-]	N [-]
PP	21.1 ± 7.3	9.9 ± 0.7	0.332 ± 0.047	33.1 ± 5.8	1.48	0.970	27
PP/2.5BA80	31.1 ± 7.8	9.0 ± 0.8	0.275 ± 0.067	44.9 ± 12.3	1.88	0.963	25
PP/5BA80	31.5 ± 6.8	8.9 ± 0.7	0.310 ± 0.034	30.7 ± 4.5	2.25	0.969	25
PP/10BA80	24.4 ± 5.3	8.9 ± 0.5	0.286 ± 0.033	33.3 ± 4.9	1.49	0.981	26
PP/2.5BA80-OS	26.3 ± 5.8	9.7 ± 0.6	0.304 ± 0.044	35.3 ± 6.1	1.78	0.979	26
PP/5BA80-OS	23.8 ± 7.7	9.1 ± 0.7	0.302 ± 0.041	33.3 ± 5.7	1.54	0.966	25
PP/10BA80-OS	22.7 ± 3.9	8.8 ± 0.4	0.304 ± 0.030	30.3 ± 3.6	1.60	0.989	27
PP/2.5BA80-OS2	24.1 ± 6.7	8.5 ± 0.7	0.321 ± 0.060	31.7 ± 7.0	1.60	0.967	24

Figure 1

(a)

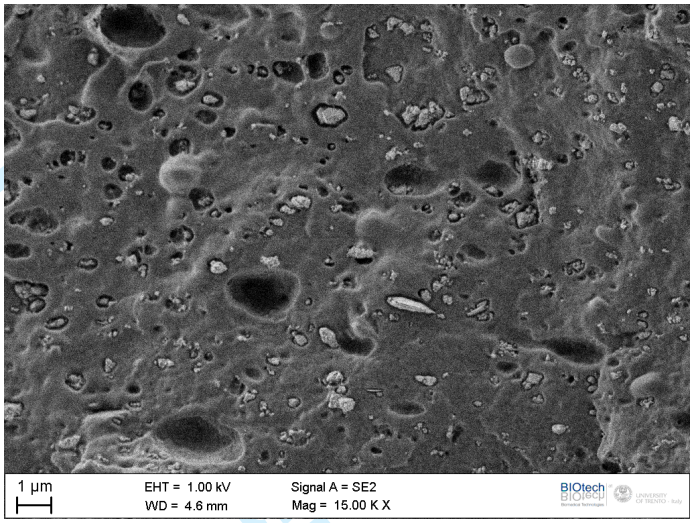
1 µm
EHT = 1.00 kV
WD = 4.6 mm
Signal A = SE2
Mag = 15.00 K X
BIOtech

(b)

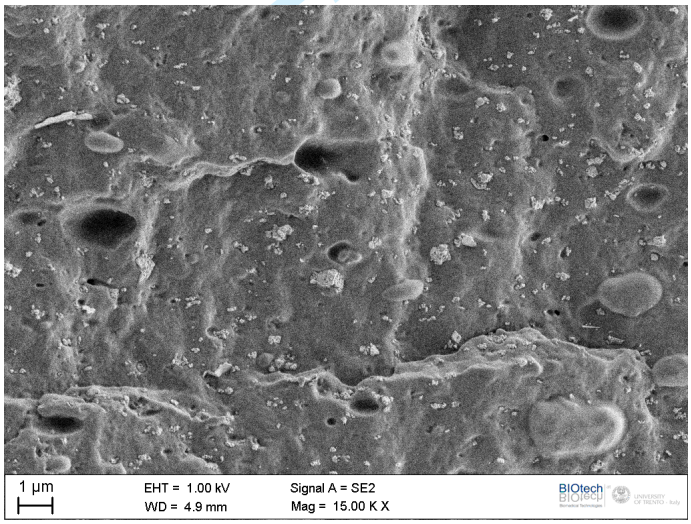
1 µm
EHT = 1.00 kV
WD = 4.9 mm
Signal A = SE2
Mag = 15.00 K X
BIOtech

(c)

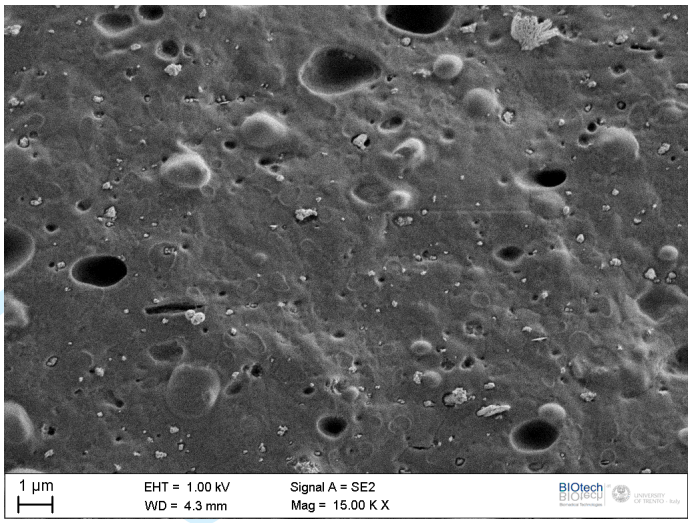

Figure 2

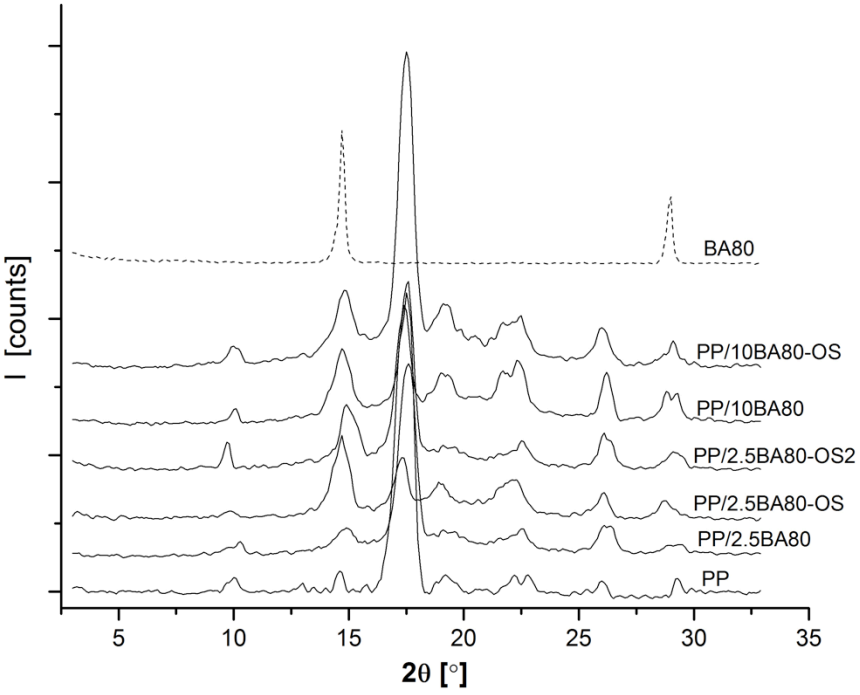
I [counts]
2θ [°]
5
10
15
20
25
30
35
BA80
PP/10BA80-OS
PP/10BA80
PP/2.5BA80-OS2
PP/2.5BA80-OS
PP/2.5BA80
PP

Figure 3

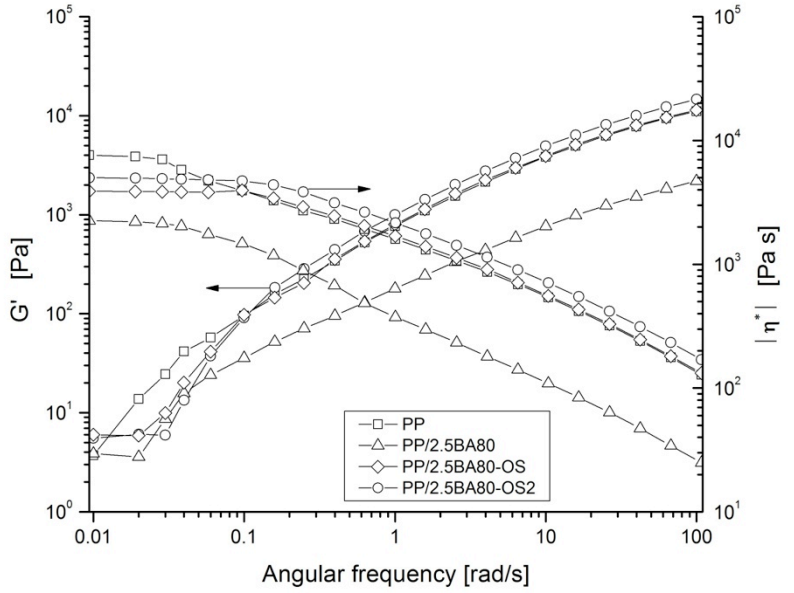
G' [Pa]
|η*| [Pa s]
Angular frequency [rad/s]
PP
PP/2.5BA80
PP/2.5BA80-OS
PP/2.5BA80-OS2

(a)

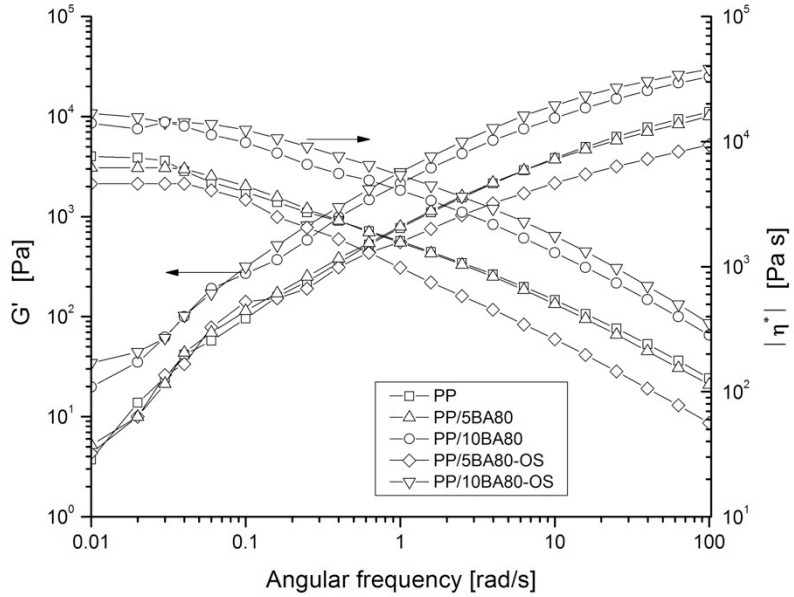
G' [Pa]
|η*| [Pa s]
Angular frequency [rad/s]
PP
PP/5BA80
PP/10BA80
PP/5BA80-OS
PP/10BA80-OS

(b)

Figure 4

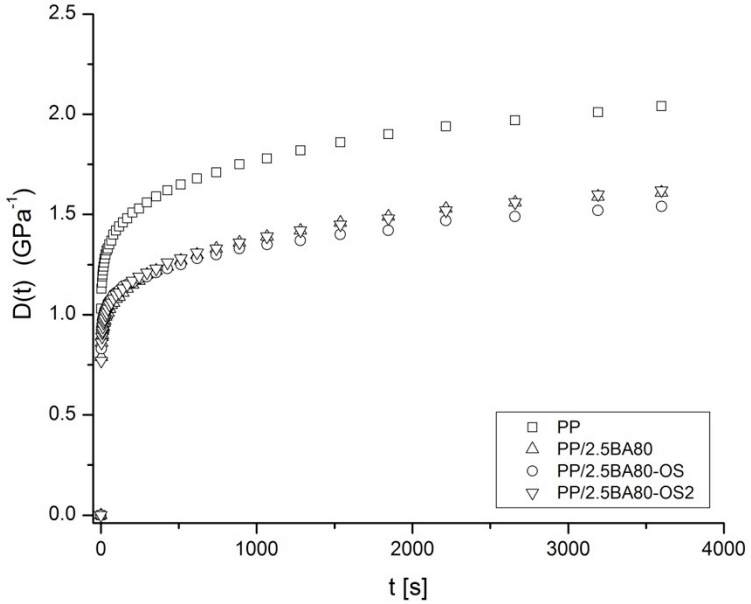
D(t) (GPa^{-1})
t [s]
PP
PP/2.5BA80
PP/2.5BA80-OS
PP/2.5BA80-OS2

(a)

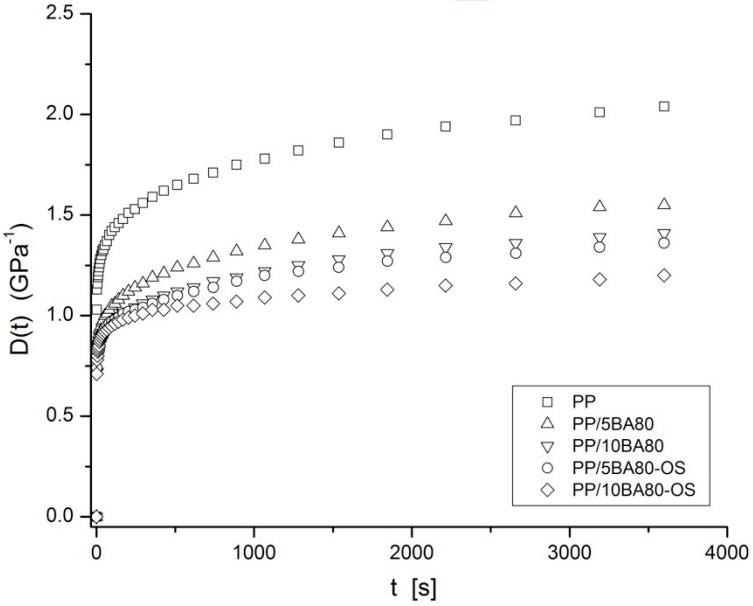
D(t) (GPa^{-1})
t [s]
PP
PP/5BA80
PP/10BA80
PP/5BA80-OS
PP/10BA80-OS

(b)

Figure 5

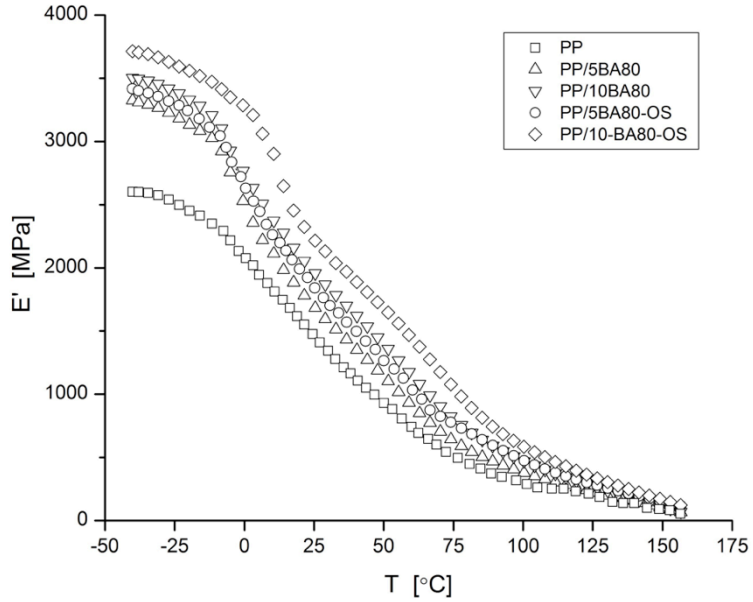
PP
PP/5BA80
PP/10BA80
PP/5BA80-OS
PP/10-BA80-OS
E' [MPa]
T [°C]

(a)

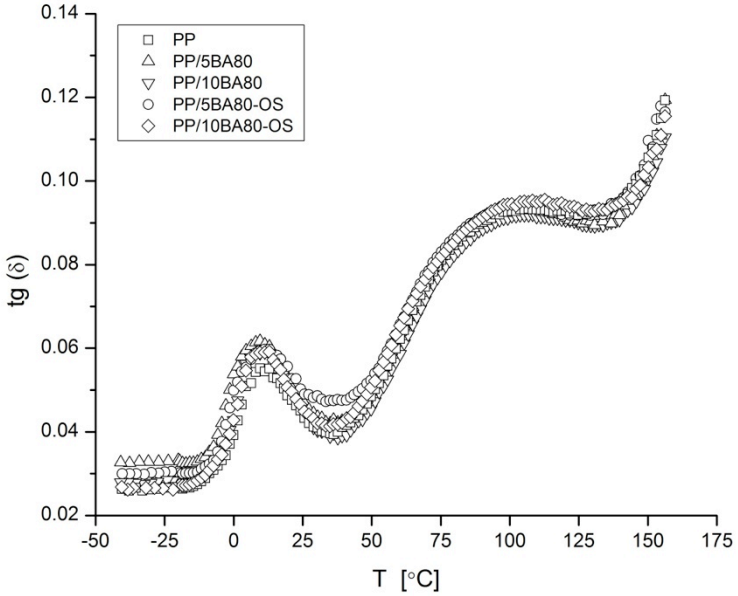
PP
PP/5BA80
PP/10BA80
PP/5BA80-OS
PP/10BA80-OS
tg (δ)
T [°C]

(b)

Figure 6

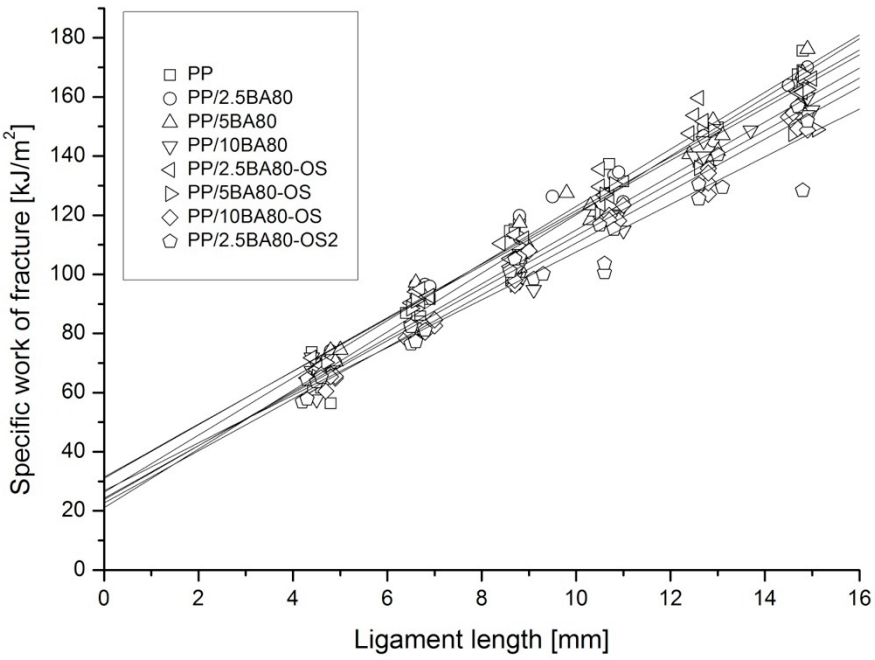

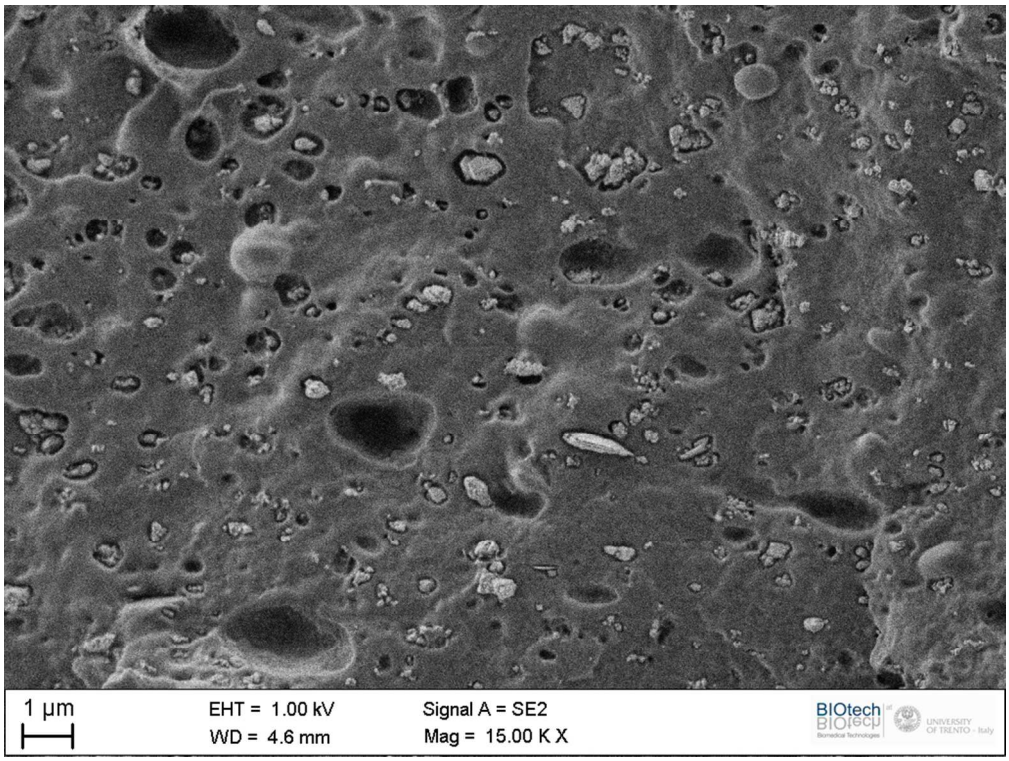

361x270mm (72 x 72 DPI)

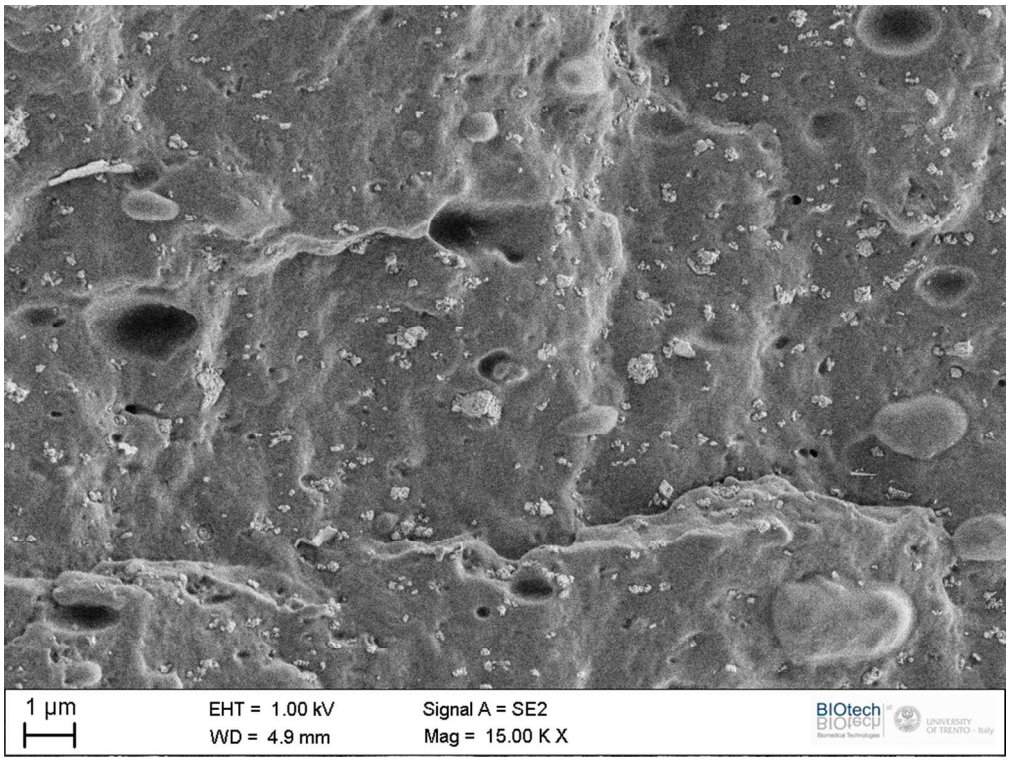

26009x19507mm (1 x 1 DPI)

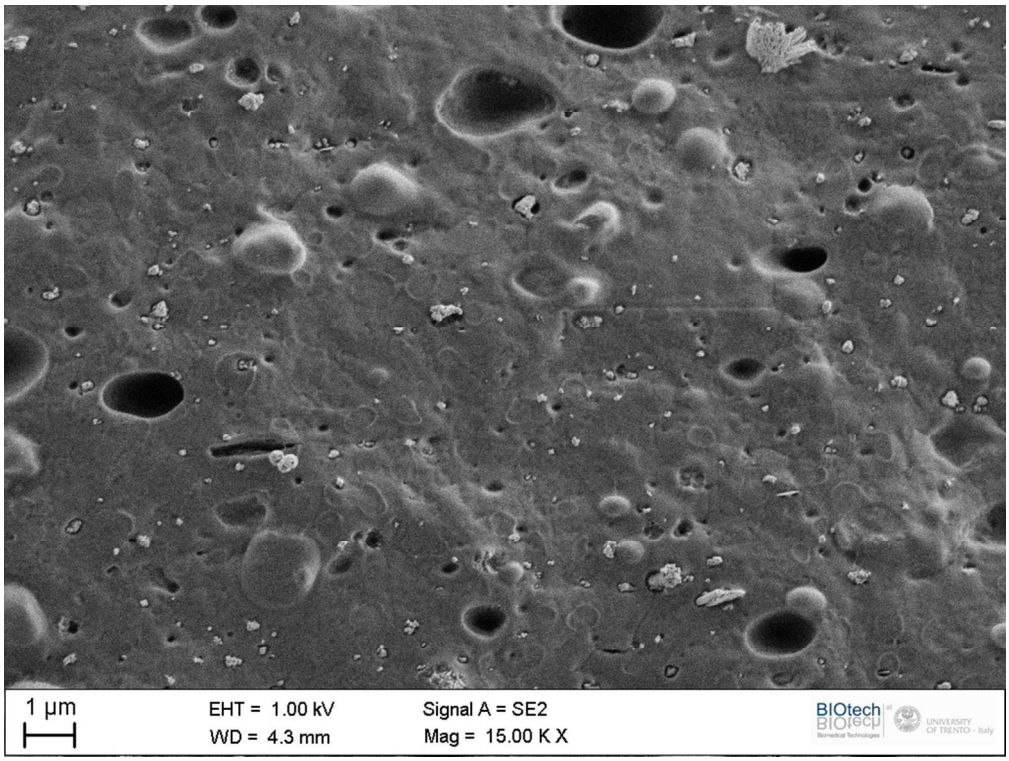

26009x19507mm (1 x 1 DPI)

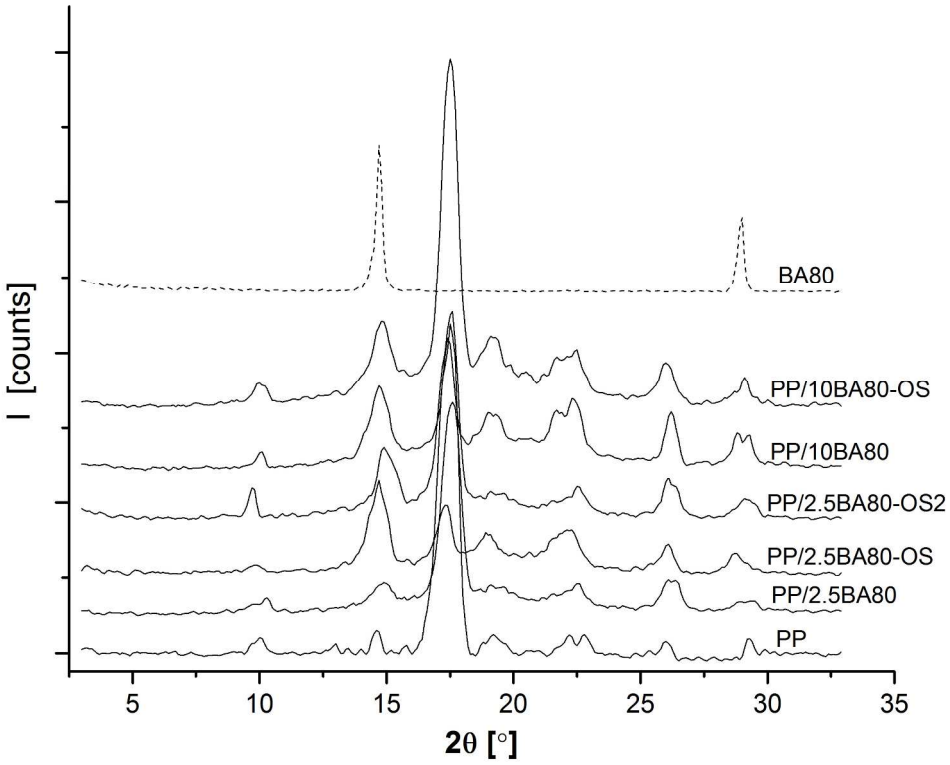

224x174mm (300 x 300 DPI)

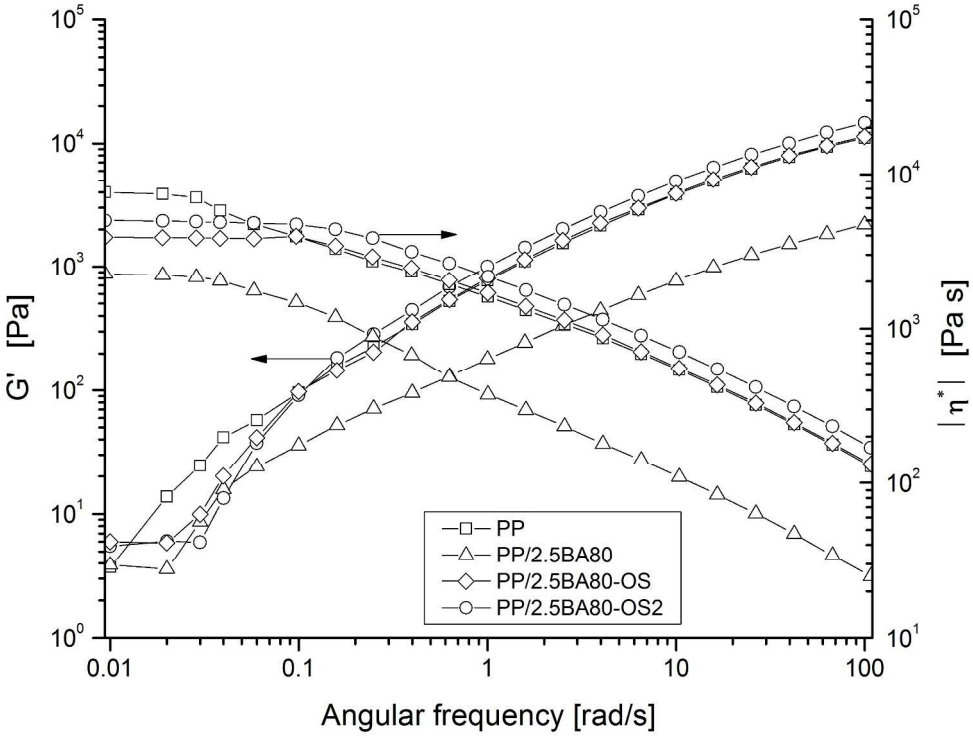

241x181mm (300 x 300 DPI)

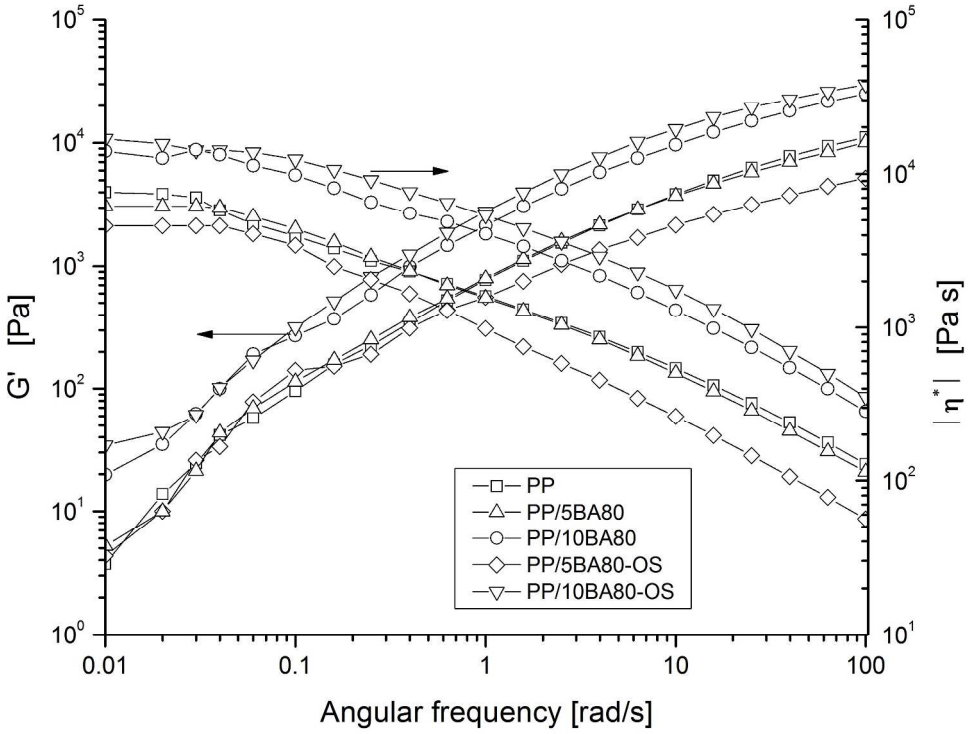

242x179mm (300 x 300 DPI)

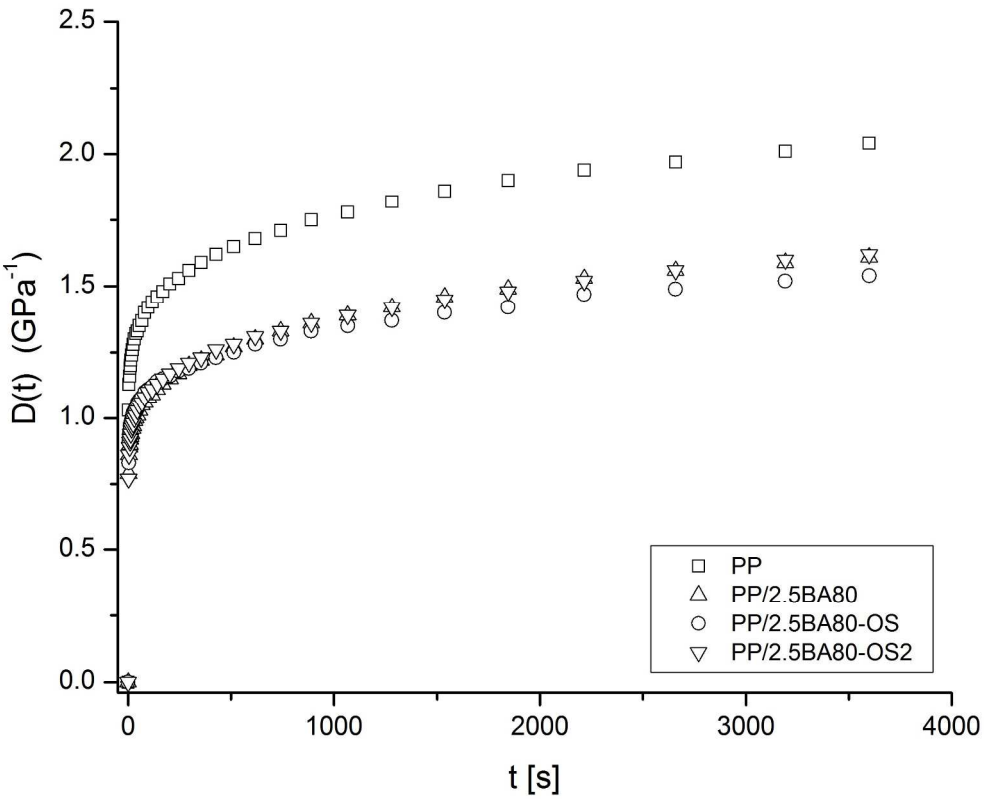

221x176mm (300 x 300 DPI)

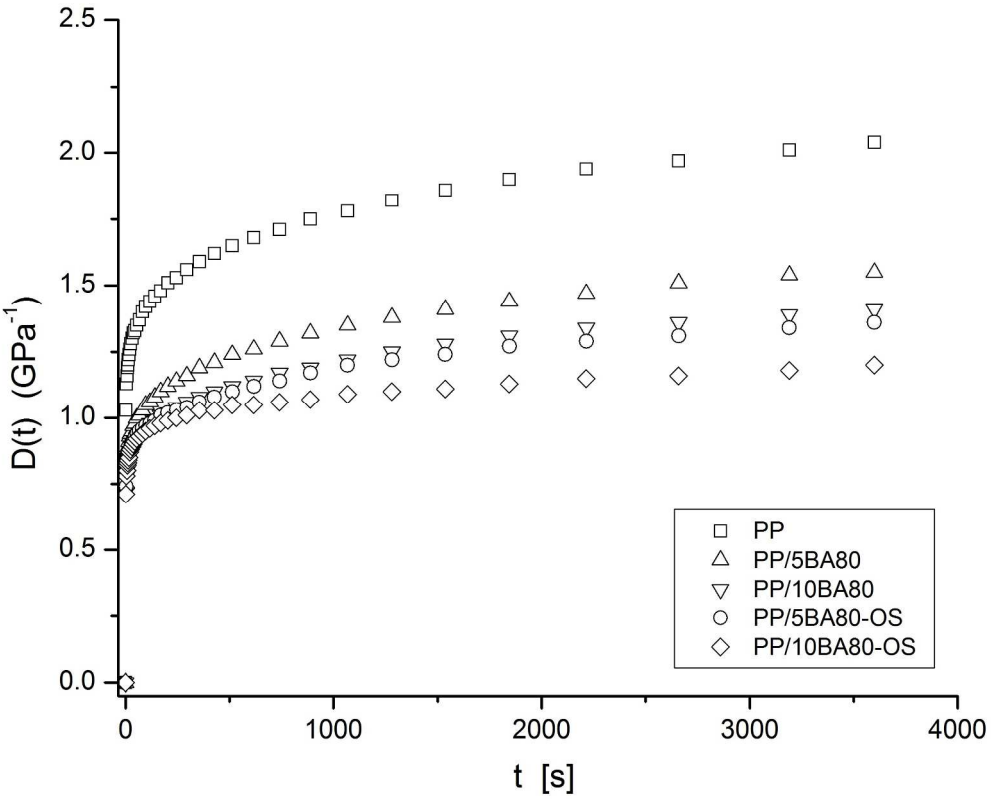

220x175mm (300 x 300 DPI)

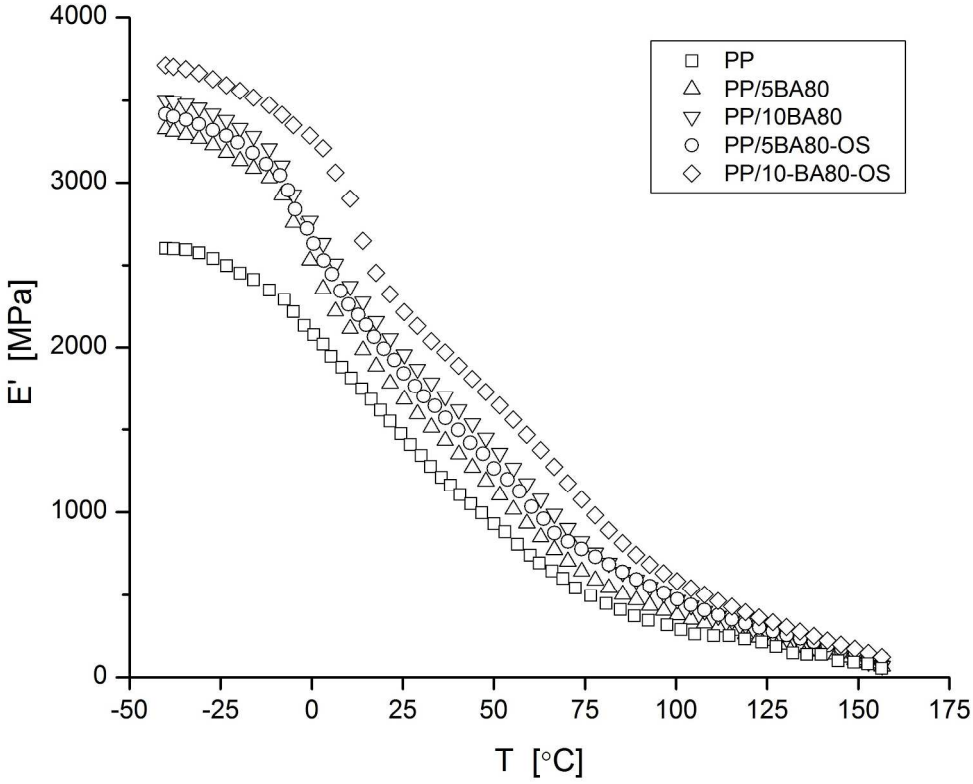

225x178mm (300 x 300 DPI)

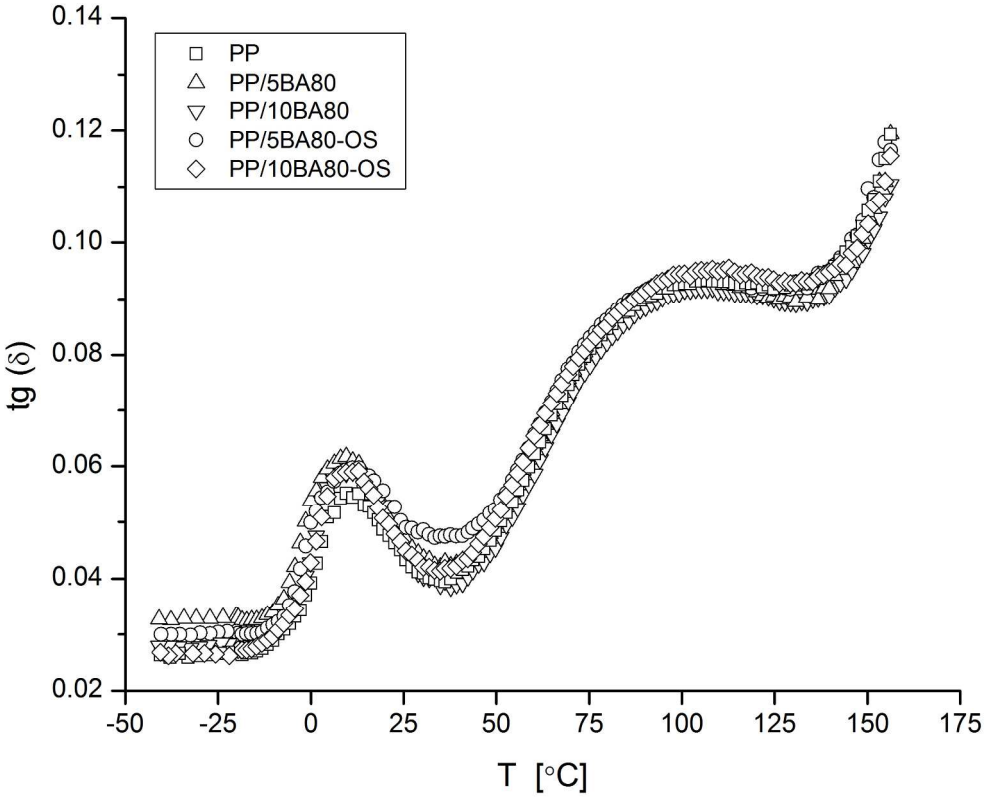

221x179mm (300 x 300 DPI)

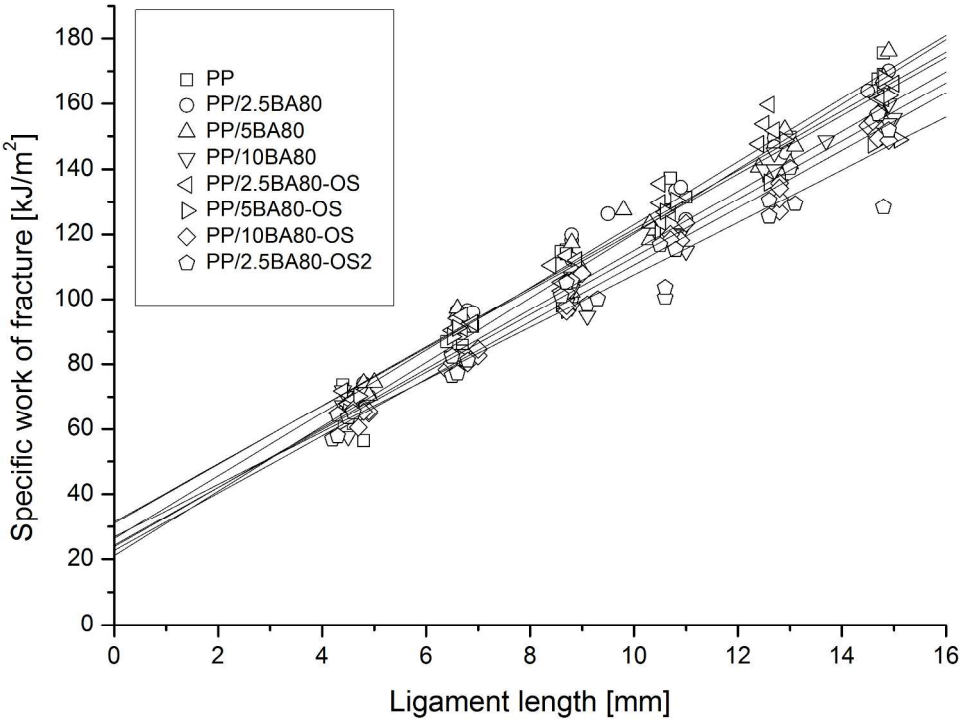

243x180mm (300 x 300 DPI)